Original Article | Thoracic Imaging

https://doi.org/10.3348/kjr.2018.19.3.516
pISSN 1229-6929 · eISSN 2005-8330
Korean J Radiol 2018;19(3):516-525

Korean Journal of Radiology
KJR

Nodule Classification on Low-Dose Unenhanced CT and Standard-Dose Enhanced CT: Inter-Protocol Agreement and Analysis of Interchangeability

Kyung Hee Lee, MD[1], Kyung Won Lee, MD[1], Ji Hoon Park, MD[1], Kyunghwa Han, PhD[2], Jihang Kim, MD[1], Sang Min Lee, MD[3], Chang Min Park, MD[4, 5]

[1]Department of Radiology, Seoul National University Bundang Hospital, Seongnam 13620, Korea; [2]Department of Radiology, Research Institute of Radiological Science, Yonsei University College of Medicine, Seoul 03722, Korea; [3]Department of Radiology and Research Institute of Radiology, University of Ulsan College of Medicine, Asan Medical Center, Seoul 05505, Korea; [4]Department of Radiology, Seoul National University Hospital, Seoul National University College of Medicine, Seoul 03080, Korea; [5]Cancer Research Institute, Seoul National University College of Medicine, Seoul 03080, Korea

Objective: To measure inter-protocol agreement and analyze interchangeability on nodule classification between low-dose unenhanced CT and standard-dose enhanced CT.

Materials and Methods: From nodule libraries containing both low-dose unenhanced and standard-dose enhanced CT, 80 solid and 80 subsolid (40 part-solid, 40 non-solid) nodules of 135 patients were selected. Five thoracic radiologists categorized each nodule into solid, part-solid or non-solid. Inter-protocol agreement between low-dose unenhanced and standard-dose enhanced images was measured by pooling κ values for classification into two (solid, subsolid) and three (solid, part-solid, non-solid) categories. Interchangeability between low-dose unenhanced and standard-dose enhanced CT for the classification into two categories was assessed using a pre-defined equivalence limit of 8 percent.

Results: Inter-protocol agreement for the classification into two categories {κ, 0.96 (95% confidence interval [CI], 0.94–0.98)} and that into three categories (κ, 0.88 [95% CI, 0.85–0.92]) was considerably high. The probability of agreement between readers with standard-dose enhanced CT was 95.6% (95% CI, 94.5–96.6%), and that between low-dose unenhanced and standard-dose enhanced CT was 95.4% (95% CI, 94.7–96.0%). The difference between the two proportions was 0.25% (95% CI, -0.85–1.5%), wherein the upper bound CI was markedly below 8 percent.

Conclusion: Inter-protocol agreement for nodule classification was considerably high. Low-dose unenhanced CT can be used interchangeably with standard-dose enhanced CT for nodule classification.

Keywords: *Pulmonary nodules; Classification; Subsolid nodule; Ground-glass nodule; Computed tomography; Low-dose CT*

Received August 23, 2017; accepted after revision November 13, 2017.

This study was supported by a grant of the Korean Health Technology R&D Project, Ministry of Health & Welfare, Republic of Korea (HI14C2175).

Corresponding author: Kyung Won Lee, MD, Department of Radiology, Seoul National University Bundang Hospital, 82 Gumi-ro 173beon-gil, Bundang-gu, Seongnam 13620, Korea.
• Tel: (8231) 787-7604 • Fax: (8231) 787-4011
• E-mail: lkwrad@gmail.com

INTRODUCTION

It is crucial to classify pulmonary nodules accurately and reliably to ensure that appropriate clinical decisions are made both in routine practice and in the screening setting. For incidentally detected nodules, different guideline algorithms are being applied for solid and subsolid nodules according to the Fleischner Society guideline (1). For nodules detected on lung cancer screening, Lung CT Screening Reporting and Data System indicates varying patient management according to the classification of pulmonary nodules into solid, part-solid and non-solid

Korean Journal of Radiology
KJR

nodules on low-dose CT (2).

Since the National Lung Screening Trial reported a 20% reduction in lung cancer mortality among high-risk populations, low-dose chest CT has received increased attention and has been in widespread use for routine practice as well as lung cancer screening (3). However, there is a growing concern because a fair amount of inter- and intra-observer variability exists in nodule classification on low-dose CT, which may lead to different patient management (4, 5). Preceding research has reported comparable accuracy between low-dose and standard-dose chest CT for nodule detection and size measurement (6-9). However, it is unclear whether nodule classification on low-dose CT can be made reliably as that on standard-dose chest CT. To our knowledge, little data is available for inter-protocol agreement, which is an agreement between low-dose unenhanced and standard-dose enhanced CT for nodule classification into solid and subsolid nodules.

Diagnostic tests are typically assessed by measuring their accuracy through comparison with a reference standard (10). However, it is impossible to establish a valid reference standard in pulmonary nodule classification on CT, as the classification depends on each reader's subjective visual assessment (4, 5, 11). With a method suggested by Obuchowski, the interchangeability of low-dose unenhanced CT with standard-dose enhanced CT can be investigated by comparing agreement in classifications between the two CT protocols to the agreement between readers with standard-dose enhanced CT (10, 12). Accordingly, we aimed to measure inter-protocol agreement and analyze interchangeability on nodule classification between low-dose (0.5-mSv) unenhanced CT and standard-dose (4.5-mSv) enhanced CT.

MATERIALS AND METHODS

This retrospective study was approved by our Institutional Review Board (B-1604/343-116), and the need for informed consent was waived.

Nodule Selection

Solid and subsolid nodule libraries containing both low-dose unenhanced and standard-dose enhanced CT images were established using the electronic radiology database of our institution by a single chest radiologist. Long and short diameters of the nodules were measured using an electronic caliper on axial images, and the locations of the nodules were recorded as upper, middle, or lower, by dividing the lungs into three areas (13).

To identify eligible solid and subsolid nodules for the nodule libraries, different search terms and periods were used to adjust for the difference in the prevalence of solid and subsolid nodules. In our institution, low-dose unenhanced chest CT has been included in the contrast-enhanced chest CT protocol since 2008 in order to obtain information on the degree of contrast enhancement and the presence of calcification, which provides essential data needed to differentiate between benign and malignant lesions, particularly in tuberculosis-endemic countries (7, 14). Patients underwent contrast-enhanced chest CT protocol for various reasons, including clinical symptoms, chest radiography abnormality, or staging purposes.

To identify eligible CT images of solid nodules, 1269 consecutive contrast-enhanced CT images obtained over 4 months were reviewed. To identify eligible CT images of subsolid nodules, 6747 consecutive contrast-enhanced CT reports over 2 years were searched to identify CT reports which contained terms indicating subsolid nodules. The solid and subsolid nodules that met the following inclusion criteria were identified: average diameter ≥ 6 mm; no calcification or ossification; no satellite nodule; no disseminated lesion; and no perceptible motion artifact. The nodules with satellite lesions were excluded because they are much more common in solid nodules (i.e., pulmonary tuberculosis). These selected nodules were reviewed together by two chest radiologists (with 4 and 14 years of experience, respectively) to classify the nodules in consensus. Finally, a solid nodule library comprising 208 nodules and a subsolid nodule library comprising 126 nodules were established. Among these, 80 solid nodules and 80 subsolid nodules (including 40 part-solid and 40 non-solid nodules) of 135 patients were selected for the study via random sampling, and stratified by nodule size (Fig. 1). There were 72 male patients (mean age, 65.1 years ± 11.9; age range, 27–86 years) and 63 female patients (mean age, 67.3 years ± 11.9; age range, 44–91 years). The median body weight and body mass index of our study patients were 56 kg (interquartile range [IQR], 50.3–65.5 kg) and 22.5 kg/m^2 (IQR, 20.4–24.6 kg/m^2), respectively.

CT Image Acquisition

All CT images were obtained using 256-slice multi-detector row scanners (iCT; Philips Medical Systems, Cleveland, OH, USA). The target radiation doses for the low-

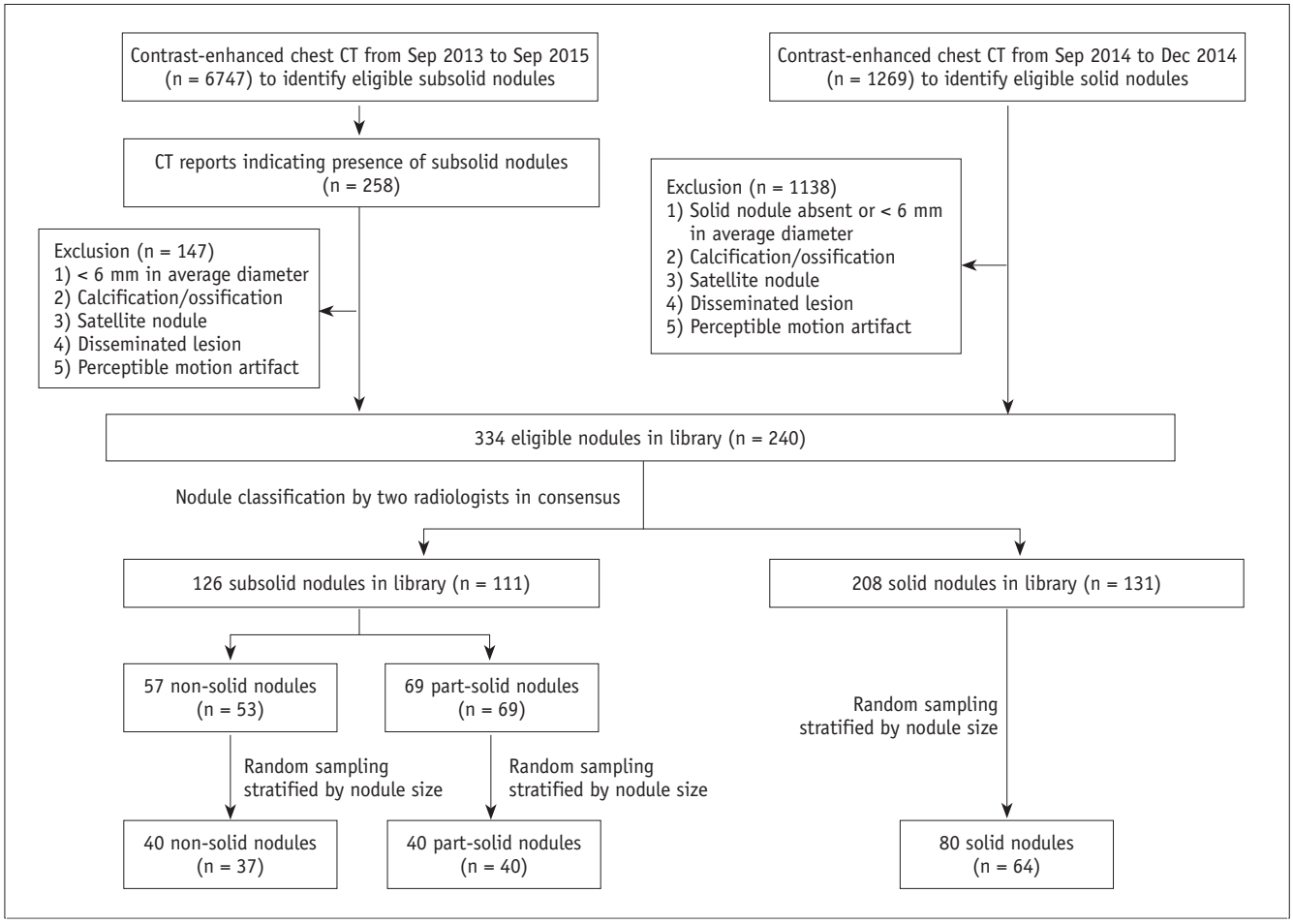

Fig. 1. Flowchart of nodule selection. Numbers in parentheses represent number of patients.

dose unenhanced and standard-dose enhanced images were 0.5 mSv and 4.5 mSv, respectively.

Low-dose unenhanced CT was performed at a tube potential of 120 kVp with automatic exposure control (DoseRight index 4 [average mAs of 21]), beam collimation of 128 x 0.625 mm, pitch of 0.984, and gantry rotation time of 0.5 seconds before the intravenous injection of contrast material. Contrast agent (80 mL; iomeprol, Iomeron 350; Bracco, Buckinghamshire, UK) was injected intravenously at a rate of 2–3 mL/s via automatic power injection. The subsequent standard-dose enhanced chest CT was acquired 30 seconds after achieving a threshold of 200 Hounsfield unit (HU) in the ascending aorta via the bolus-tracking technique. All the parameters remained unchanged, except the setting of automatic exposure control (DoseRight index 18 [average mAs of 101]). Images were reconstructed using a filtered back projection algorithm with a sharp convolution kernel (YA), with 1 mm section thickness and 1 mm interval. Radiation doses were estimated by using volumetric CT dose index (CTDIvol), size-specific dose estimates (SSDEs), and effective dose. SSDEs were calculated using the method described in the American Association of Physicists in Medicine task group report 204 (15), based on the effective diameter of each patient at the level of the tracheal bifurcation (16). We estimated the effective dose by using a conversion factor of 0.014 mSv/mGy·cm, as reported in Report 96 of the American Association of Physicists in Medicine (17).

Image Analysis

Five chest radiologists from four different institutions (with 20, 16, 8, 6, and 2 years of experience, respectively) participated in nodule classification. All axial CT images that contained nodules were provided along with the lung window settings (level, -600 HU; width, 1500 HU). The readers were instructed to categorize each nodule into solid or subsolid, and to further subcategorize the subsolid nodules into part-solid or non-solid. Classification was based on the definition by the Fleischner Society (18, 19) and no further discussion was made to refine

Korean Journal of Radiology
KJR

these definitions. The readers were blinded to the original classification in the CT reports, the number of nodules in each category, and the findings of the other radiologists. If needed, the readers were allowed to adjust the window settings and magnification.

Each reader reviewed the CT scans of each nodule twice, once with low-dose unenhanced CT and once with standard-dose enhanced chest CT during two reading sessions: each session included 80 low-dose unenhanced and 80 standard-dose enhanced images, randomly mixed, and repetition of any nodule in a single session was avoided. The maximal number of review cases was limited to 40 per day. There was at least a 6-week time interval between the first and second sessions to reduce the potential for recall bias.

Statistical Analysis

Inter-protocol and inter-reader agreement were measured for nodule classification into two (solid versus subsolid) and three (solid, part-solid, versus non-solid) categories. Inter-protocol agreement was calculated by pooling each reader's agreement between low-dose unenhanced CT and standard-dose enhanced CT, using the proportion of agreement and Cohen's kappa (κ) statistics (20). Inter-reader agreement on low-dose unenhanced and on standard-dose enhanced images was calculated using the proportion of agreement and Fleiss' kappa (21). Subgroup analysis was performed by dividing the nodules into three subgroups according to size and location, with logistic regression using the generalized estimating equation method.

The interchangeability between low-dose unenhanced and standard-dose enhanced CT images for classification into solid and subsolid nodules was tested using the method of Obuchowski (10, 12). The equivalence limit was pre-defined as 8%, which was the median value of the intra-reader disagreement among experienced thoracic radiologists for nodule classification in a previous study (11). The individual equivalence index (IEC) was calculated by subtracting "the probability of agreement between the low-dose unenhanced and standard-dose enhanced CT" from "the probability of agreement between the readers with standard-dose chest CT." If the upper bound of the 95% confidence interval (CI) of the IEC was less than or equal to the equivalence limit, low-dose unenhanced chest CT would be considered to be interchangeable to standard-dose enhanced chest CT. To consider the clustered nature of the data, the 95% CI for the IEC was constructed using 10000 bootstrap samples from nodule-level data (10, 12).

All statistical analyses were performed using commercially available software (SAS version 9.4, SAS Institute Inc., Cary, NC, USA; R version 3.3.2, R Foundation for Statistical Computing, Vienna, Austria).

RESULTS

Nodule Characteristics and Radiation Doses

The 160 nodules included in our study had an average size of 12.9 mm along the long diameter (range, 6.2–29.2 mm), and were located in the upper (28.8%), middle (50.6%), and lower (20.6%) lungs. The sizes and locations of 80 solid, 40 part-solid, and 40 non-solid nodules are summarized in Table 1. The average size of the solid components in part-solid nodules was 7.3 mm (range, 2.1–17.0 mm).

In this study, the median CTDIvol and SSDEs were 1.32 mGy (IQR, 1.17–1.47 mGy) and 1.7 mGy (IQR, 1.6–1.8 mGy) for low-dose unenhanced CT, and were 7.30 mGy (IQR, 6.50–8.06 mGy) and 9.55 mGy (IQR, 8.83–10.19 mGy) for standard-dose enhanced CT, respectively. The median effective radiation dose was 0.57 mSv (IQR, 0.47–0.65 mSv) for low-dose unenhanced CT and 4.73 mSv (IQR, 3.97–5.35 mSv) for standard-dose enhanced CT.

Inter-Protocol Agreement

To provide a visual representation of the five readers'

Table 1. Nodule Characteristics

Nodule Library	No.of Nodules	Average Size (mm)*	Location (%)†		
			Upper	Middle	Lower
Solid	80	12.8 (6.3–28.2)	14 (17.5)	45 (56.3)	21 (26.2)
Subsolid					
Part-solid	40	13.6 (6.5–28.9)	17 (42.5)	15 (37.5)	8 (20.0)
Non-solid	40	12.4 (6.2–29.2)	15 (37.5)	21 (52.5)	4 (10.0)
All	160	12.9 (6.2–29.2)	46 (28.8)	81 (50.6)	33 (20.6)

*Data in parentheses indicate range, †Data represent number of nodules, whereas data in parentheses represent percentages. Locations of nodules were recorded as upper, middle, or lower by dividing lungs into three areas by aortic arch and lower pulmonary vein.

Fig. 2. Heatmap showing results of nodule classification. 160 nodules included 80 subsolid (non-solid [No. 1–40] and part-solid [No. 41–80]) and 80 solid nodules (No. 81–160) that were selected by stratified random sampling from nodule libraries. Five radiologists classified nodules as subsolid (non-solid [displayed as light green], part-solid [displayed as green],) or solid [displayed as dark green] using standard-dose enhanced and low-dose unenhanced CT images during two reading sessions. In this figure, nodules are arranged in order of increasing size in each of three classification categories, regardless of reading order and reading session.

Korean Journal of Radiology
KJR

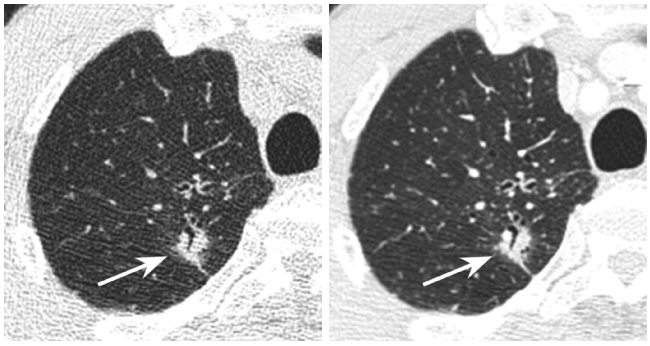

A B

Fig. 3. Axial CT images of 14.6-mm nodule in right upper lobe (No. 68).
Each of five radiologists indicated same classification for this nodule (arrows), either using low-dose unenhanced CT images **(A)** or standard dose enhanced CT images **(B)** (Reader 2–5: part-solid; Reader 1: solid).

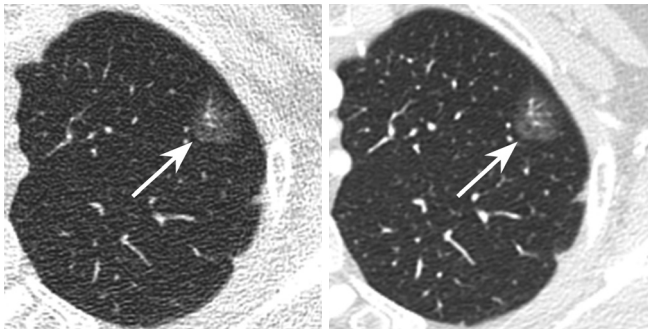

A B

Fig. 4. Axial CT images of 18-mm nodule in left upper lobe (No. 36).
A. Using low-dose unenhanced CT images, three radiologists classified nodule (arrow) as non-solid nodule, whereas two radiologists regarded this as part-solid nodule. **B.** All five of radiologists classified nodule (arrow) as non-solid nodule using standard-dose enhanced CT images.

responses, a heat map was constructed (Fig. 2) (22). Representative examples of nodule classification are shown in Figures 3 and 4. Inter-protocol agreement for the classification between solid and subsolid nodules (κ, 0.96 [95% CI, 0.94–0.98]) and that for the classification between solid, part-solid, and non-solid nodules (κ, 0.88 [95% CI, 0.85–0.92]) was considerably high. Inter-protocol agreement in classification between part-solid versus others and non-solid versus others is also shown in Table 2. Inter-protocol agreement was not associated with the size or location of the nodules ($p > 0.05$) (Table 3).

Inter-Reader Agreement

Inter-reader agreement for the classification of solid and subsolid nodules on low-dose unenhanced (κ, 0.89 [95% CI, 0.84–0.93]) and standard-dose enhanced images (κ, 0.91 [95% CI, 0.87–0.95]) was considerably high (Table 4).

Table 2. Agreement in Classification of 160 Nodules between Low-Dose Unenhanced CT and Standard-Dose Enhanced CT (Inter-Protocol Agreement)

Nodule Classification	Kappa	Proportion of Agreement (%)
Solid vs. subsolid	0.96 (0.94, 0.98)	97.1 (95.3, 98.3)
Solid vs. part-solid vs. non-solid	0.88 (0.85, 0.92)	92.1 (89.5, 94.2)
Part-solid vs. others	0.91 (0.89, 0.94)	92.3 (89.6, 94.3)
Non-solid vs. others	0.95 (0.95, 0.97)	94.9 (92.4, 96.6)

Agreement for each of five readers on nodule classification between low-dose unenhanced CT and standard-dose enhanced CT was pooled. 95% CIs for each point estimate are shown in parentheses. CIs = confidence intervals

Agreement for the classification of solid, part-solid, and non-solid nodules on low-dose unenhanced (κ, 0.82 [95% CI, 0.77–0.87]) and standard-dose enhanced images (κ, 0.87 [95% CI, 0.83–0.91]) was also markedly high. There was no significant difference in inter-reader agreement between low-dose unenhanced and standard-dose enhanced images.

Inter-reader agreement was not associated with nodule size or location (Table 5), with the exception of the inter-reader agreement for classification between solid and subsolid nodules, which tended to decrease slightly in larger-sized nodules on low-dose unenhanced CT images ($p = 0.03$) and standard-dose enhanced CT ($p = 0.06$). In nodules larger than 20 mm, the Fleiss' kappa values for the classification between solid and subsolid nodules were 0.74 (95% CI, 0.51–0.94) and 0.74 (95% CI, 0.48–0.95) on low-dose unenhanced CT and standard-dose enhanced CT, respectively.

Interchangeability Test

The probability of agreement between readers on standard-dose enhanced CT was 95.6% (95% CI, 94.5–96.6%), and the probability of agreement between the low-dose unenhanced and standard-dose enhanced CT was 95.4% (95% CI, 94.7–96.0%). The difference between the two proportions, the IEC, was 0.25% (95% CI, -0.85–1.5%). As the upper bound of CI of the IEC was markedly below the pre-defined equivalence limit of 8%, the interchangeability between low-dose unenhanced and standard-dose enhanced CT was accepted.

DISCUSSION

There has been a marked increase in the use of low-dose CT for lung cancer screening and routine practice.

Table 3. Agreement in Nodule Classification between Low-Dose Unenhanced CT and Standard-Dose Enhanced CT (Inter-Protocol Agreement) according to Nodule Size and Location

	Kappa	Proportion of Agreement (%)	*P**
Size			
Solid vs. subsolid			0.31
Size ≤ 10 mm	0.98 (0.96, 1.00)	98.6 (95.5, 99.6)	
10 mm < size ≤ 20 mm	0.95 (0.92, 0.98)	96.1 (93.1, 97.9)	
20 mm < size ≤ 30 mm	0.97 (0.93, 1.00)	97.5 (91.2, 99.3)	
Solid vs. part-solid vs. non-solid			0.87
Size ≤ 10 mm	0.89 (0.83, 0.94)	92.1 (87.0, 95.4)	
10 mm < size ≤ 20 mm	0.88 (0.83, 0.93)	91.8 (88.0, 94.5)	
20 mm < size ≤ 30 mm	0.89 (0.80, 0.98)	93.8 (85.0, 97.6)	
Location			
Solid vs. subsolid			0.62
Upper	0.98 (0.96, 1.00)	98.3 (95.6, 99.3)	
Middle	0.95 (0.91, 0.99)	96.3 (92.9, 98.1)	
Lower	0.96 (0.92, 1.00)	97.6 (94.0, 99.0)	
Solid vs. part-solid vs. non-solid			0.15
Upper	0.85 (0.78, 0.92)	89.1 (82.7, 93.4)	
Middle	0.89 (0.84, 0.94)	93.1 (89.3, 95.6)	
Lower	0.89 (0.83, 0.96)	93.9 (88.6, 96.9)	

Agreement for each of five readers on nodule classification between low-dose unenhanced CT and standard-dose enhanced CT was pooled. 95% CIs for each point estimate are shown in parentheses. *Logistic regression using generalized estimating equation method was performed to determine whether agreement differed according to nodule size or location. *p* value < 0.05 indicates statistical significance.

Table 4. Inter-Reader Agreement for Nodule Classification on Low-Dose Unenhanced CT and Standard-Dose Enhanced CT

	Fleiss' Kappa	Proportion of Agreement (%)	*P**
Solid vs. subsolid			0.25
Low-dose unenhanced CT	0.89 (0.84, 0.93)	87.5 (82.4, 92.6)	
Standard-dose enhanced CT	0.91 (0.87, 0.95)	90.0 (85.4, 94.7)	
Solid vs. part-solid vs. non-solid			0.12
Low-dose unenhanced CT	0.82 (0.77, 0.87)	76.2 (69.7, 82.8)	
Standard-dose enhanced CT	0.87 (0.83, 0.91)	81.9 (75.9, 87.8)	

Fleiss' kappa and proportion of agreement were measured when all of five readers agreed on classification. 95% CIs for each point estimate are shown in parentheses. *Logistic regression using generalized estimating equation method was performed to evaluate whether there was difference between inter-reader agreement on low-dose unenhanced and standard-dose enhanced CT. *p* value < 0.05 indicates statistical significance.

To determine whether nodule classification on low-dose unenhanced CT can be made reliably as that on standard-dose enhanced chest CT, we investigated inter-protocol agreement for nodule classification and analyzed interchangeability between low-dose unenhanced CT and standard-dose enhanced CT. Our findings strongly suggest that low-dose unenhanced CT (0.5-mSv) can be used interchangeably with standard-dose enhanced CT (4.5-mSv) in patient management based on classification between solid and subsolid nodules. Switching between low-dose unenhanced and standard-dose enhanced CT only leads to a negligible change in agreement regarding nodule classification (within the range of a 0.85% decrease and 1.5% increase), from that using standard-dose enhanced CT alone.

The agreement for nodule classification in the present study tended to be higher than those reported in previous studies, wherein the inter-reader agreement (κ) was 0.51–0.81 and intra-reader agreement (κ) was 0.57–0.79 (4, 5, 11). This discrepancy could be explained by several differences among the studies. First, the proportions of solid and subsolid nodules were different. The proportion of subsolid nodules was higher in the previous studies (67% in the study by Jacobs et al. (4) and 75% in the study by van Riel et al. (5) than that in our study (50%). Since disagreement on the size and presence of a solid component

Korean Journal of Radiology
KJR

Table 5. Inter-Reader Agreement for Nodule Classification on Low-Dose Unenhanced CT and Standard-Dose Enhanced CT Images, according to Nodule Size and Location

	Fleiss' Kappa	Proportion of Agreement (%)	*P**
Size			
Solid vs. subsolid			
Low-dose unenhanced CT			0.03
Size ≤ 10 mm	0.96 (0.90, 1.00)	94.6 (88.8, 100)	
10 mm < size ≤ 20 mm	0.87 (0.79, 0.93)	85.2 (77.8, 92.6)	
20 mm < size ≤ 30 mm	0.74 (0.51, 0.94)	75.0 (53.8, 96.2)	
Standard-dose enhanced CT			0.06
Size ≤ 10 mm	0.94 (0.87, 0.99)	92.9 (86.1, 99.6)	
10 mm < size ≤ 20 mm	0.93 (0.87, 0.97)	90.9 (84.9, 96.9)	
20 mm < size ≤ 30 mm	0.74 (0.48, 0.95)	75.0 (53.8, 96.2)	
Solid vs. part-solid vs. non-solid			
Low-dose unenhanced CT			0.57
Size ≤ 10 mm	0.87 (0.80, 0.93)	82.1 (72.1, 92.2)	
10 mm < size ≤ 20 mm	0.82 (0.74, 0.88)	75.0 (66.0, 84.1)	
20 mm < size ≤ 30 mm	0.67 (0.44, 0.86)	62.5 (38.8, 86.2)	
Standard-dose enhanced CT			0.90
Size ≤ 10 mm	0.88 (0.80, 0.94)	82.1 (72.1, 92.2)	
10 mm < size ≤ 20 mm	0.89 (0.84, 0.94)	84.1 (76.5, 91.7)	
20 mm < size ≤ 30 mm	0.72 (0.45, 0.91)	68.8 (46.0, 91.5)	
Location			
Solid vs. subsolid			
Low-dose unenhanced CT			0.57
Upper	0.87 (0.74, 0.97)	89.1 (80.1, 98.1)	
Middle	0.89 (0.81, 0.95)	87.7 (80.5, 94.8)	
Lower	0.87 (0.76, 0.97)	84.9 (72.6, 97.1)	
Standard-dose enhanced CT			0.90
Upper	0.87 (0.75, 0.96)	87.0 (77.2, 96.7)	
Middle	0.94 (0.88, 0.98)	92.6 (86.9, 98.3)	
Lower	0.89 (0.76, 0.98)	87.9 (76.7, 99.0)	
Solid vs. part-solid vs. non-solid			
Low-dose unenhanced CT			0.76
Upper	0.78 (0.67, 0.87)	69.6 (56.3, 82.9)	
Middle	0.85 (0.78, 0.91)	81.5 (73.0, 89.9)	
Lower	0.78 (0.65, 0.89)	72.7 (57.5, 87.9)	
Standard-dose enhanced CT			0.14
Upper	0.82 (0.72, 0.90)	74.0 (61.2, 86.6)	
Middle	0.88 (0.82, 0.94)	84.0 (76.0, 91.9)	
Lower	0.90 (0.78, 0.98)	87.9 (76.7, 99.0)	

Fleiss' kappa and proportion of agreement were measured when all five readers agreed on classification. 95% CIs for each point estimate are shown in parentheses. *Logistic regression was performed to determine whether agreement differed according to nodule size or location. *p* value < 0.05 indicates statistical significance.

in subsolid nodules was the main cause of discrepancies in nodule classification (5), higher proportions of subsolid nodules in the previous studies might have resulted in lower levels of agreement (4, 5). In the study by Ridge et al. (11), the proportion of subsolid nodules was the same as in our study. However, one single CT image was provided per nodule, which may have decreased diagnostic performance in their study. In our study, all involved CT sections containing nodules were provided to reflect the clinical practice. Second, the study by van Riel et al. (5) classified nodules into four categories. In the present study, we did not incorporate the subcategories based

on size measurement, as each guideline (2, 19, 23, 24) applies different size criteria for the subcategories. Third, the nodules characteristics, such as the margin and attenuation, may be different because the nodules in our study were detected in clinical studies while the nodules in previous studies (4, 5) were detected in screening studies. Fourth, chest radiologists in the present study might have been more familiar with differentiating between solid and subsolid nodules, since subsolid nodules are more frequently found in Asian patients (25). Indeed, Lee et al. (26) reported high inter-reader agreement (κ, 0.86) for classification of part-solid and non-solid nodules, consistent with the present study. Finally, because there was no exclusion criterion for CT images with motion artifact, there is a possibility that some CT images with motion artifact were included in previous studies (4, 5), which may have decreased the degree of agreement.

In the present study, we examined the interchangeability between low-dose unenhanced and standard-dose enhanced CT for nodule classification into the two categories of solid and subsolid. Although the interchangeability test was not performed for the classification of nodules into the three categories of solid, part-solid and non-solid, nodule classification on low-dose unenhanced CT into the three categories indicated considerable agreement with that on standard-dose enhanced CT, as well as with the classification into the two categories.

The classification of pulmonary nodules depends on visual assessment, which may be affected by the nodule characteristics and lung lesion conspicuity (27). In the subgroup analysis, inter-reader agreement for the classification between solid and subsolid nodules tended to decrease slightly in nodules with larger sizes. When a minimal degree of ground-glass opacities was found to be surrounding the nodules, the classification of these nodules as solid or subsolid varied among readers, particularly for nodules > 20 mm. Iterative reconstruction is one of the important factors influencing lesion conspicuity. Without the aid of iterative reconstruction, our results showed that low-dose unenhanced chest CT with filtered back projection algorithms was sufficiently interchangeable for nodule classification with standard-dose enhanced CT. Even though the effect of iterative reconstruction on nodule classification may not be substantial, it may be useful in improving image quality and enhancing nodule detection as demonstrated by previous studies (28, 29).

The present study had certain limitations which should be discussed. First, the natural prevalence of solid and subsolid nodules in actual clinical practice may differ from that in the present study. In this study, the ratio of solid to subsolid nodules was selected as 1:1, since the equivalence limit was determined based on the results from a previous study (11) wherein the prevalence of both solid and subsolid nodules was 50%. Second, our study was potentially susceptible to recall bias. To minimize this risk, we maintained at least a 6-week time interval between the first and second reading sessions. Third, the effect of contrast enhancement and radiation dose on nodule classification has not been analyzed separately. However, standard-dose enhanced chest CT was selected as a reference test in our study because it is one of the most commonly used CT protocols in clinical practice for various indications. Fourth, the effect of iterative reconstruction on nodule classification was not evaluated in this study. Fifth, since we primarily focused on interchangeability between low-dose unenhanced and standard-dose enhanced CT for nodule classification, the interchangeability of two protocols for patient management according to the Fleischner guidelines should be evaluated in future studies. Finally, a sample size calculation was not performed in the present study due to the lack of methods available which would allow us to appropriately determine the sample size for an interchangeability test (10). Hence, the sample size in this study was determined empirically, based on the previous related studies (5, 11). Nevertheless, the narrow CIs of the estimated individual equivalence indicate that the interchangeability between low-dose unenhanced CT and standard-dose enhanced CT for nodule classification can be robustly accepted.

In conclusion, inter-protocol agreement for nodule classification was considerably high. Low-dose unenhanced CT can be used interchangeably with standard-dose enhanced CT for nodule classification.

Acknowledgments

The authors would like to thank Nancy Obuchowski, Ph.D. for her advice in statistical analysis.

REFERENCES

1. MacMahon H, Naidich DP, Goo JM, Lee KS, Leung AN, Mayo JR, et al. Guidelines for management of incidental pulmonary nodules detected on CT images: from the Fleischner Society 2017. *Radiology* 2017;284:228-243
2. Lung CT screening reporting and data system (Lung-RADS).

American College of Radiology. Web site. https://www.acr.org/Clinical-Resources/Reporting-and-Data-Systems/Lung-Rads. Accessed Apr 11, 2017
3. National Lung Screening Trial Research Team, Aberle DR, Adams AM, Berg CD, Black WC, Clapp JD, et al. Reduced lung-cancer mortality with low-dose computed tomographic screening. *N Engl J Med* 2011;365:395-409
4. Jacobs C, van Rikxoort EM, Scholten ET, de Jong PA, Prokop M, Schaefer-Prokop C, et al. Solid, part-solid, or non-solid?: classification of pulmonary nodules in low-dose chest computed tomography by a computer-aided diagnosis system. *Invest Radiol* 2015;50:168-173
5. van Riel SJ, Sanchez CI, Bankier AA, Naidich DP, Verschakelen J, Scholten ET, et al. Observer variability for classification of pulmonary nodules on low-dose CT images and its effect on nodule management. *Radiology* 2015;277:863-871
6. Diederich S, Lenzen H, Windmann R, Puskas Z, Yelbuz TM, Henneken S, et al. Pulmonary nodules: experimental and clinical studies at low-dose CT. *Radiology* 1999;213:289-298
7. Gartenschläger M, Schweden F, Gast K, Westermeier T, Kauczor H, von Zitzewitz H, et al. Pulmonary nodules: detection with low-dose vs conventional-dose spiral CT. *Eur Radiol* 1998;8:609-614
8. Kim H, Park CM, Chae HD, Lee SM, Goo JM. Impact of radiation dose and iterative reconstruction on pulmonary nodule measurements at chest CT: a phantom study. *Diagn Interv Radiol* 2015;21:459-465
9. Rusinek H, Naidich DP, McGuinness G, Leitman BS, McCauley DI, Krinsky GA, et al. Pulmonary nodule detection: low-dose versus conventional CT. *Radiology* 1998;209:243-249
10. Obuchowski NA, Subhas N, Schoenhagen P. Testing for interchangeability of imaging tests. *Acad Radiol* 2014;21:1483-1489
11. Ridge CA, Yildirim A, Boiselle PM, Franquet T, Schaefer-Prokop CM, Tack D, et al. Differentiating between subsolid and solid pulmonary nodules at CT: inter- and intraobserver agreement between experienced thoracic radiologists. *Radiology* 2016;278:888-896
12. Obuchowski NA. Can electronic medical images replace hard-copy film? Defining and testing the equivalence of diagnostic tests. *Stat Med* 2001;20:2845-2863
13. Yamashiro T, Miyara T, Honda O, Kamiya H, Murata K, Ohno Y, et al. Adaptive iterative dose reduction using three dimensional processing (AIDR3D) improves chest CT image quality and reduces radiation exposure. *PLoS One* 2014;9:e105735
14. Lee SW, Kim Y, Shim SS, Lee JK, Lee SJ, Ryu YJ, et al. Image quality assessment of ultra low-dose chest CT using sinogram-affirmed iterative reconstruction. *Eur Radiol* 2014;24:817-826
15. Li B, Behrman RH. Comment on the "report of AAPM TG 204: size-specific dose estimates (SSDE) in pediatric and adult body CT examinations" [report of AAPM TG 204, 2011]. *Med Phys* 2012;39:4613-4614; author reply 4615-4616
16. Brady SL, Kaufman RA. Investigation of American Association of physicists in medicine report 204 size-specific dose estimates for pediatric CT implementation. *Radiology* 2012;265:832-840
17. McCollough C, Cody D, Edyvean S, Geise R, Gould B, Keat N, et al. *The measurement, reporting, and management of radiation dose in CT*. Virginia: American Association of Physicists in Medicine, 2008:1-34
18. Hansell DM, Bankier AA, MacMahon H, McLoud TC, Müller NL, Remy J. Fleischner society: glossary of terms for thoracic imaging. *Radiology* 2008;246:697-722
19. MacMahon H, Austin JH, Gamsu G, Herold CJ, Jett JR, Naidich DP, et al. Guidelines for management of small pulmonary nodules detected on CT scans: a statement from the Fleischner Society. *Radiology* 2005;237:395-400
20. Yang Z, Zhou M. Kappa statistic for clustered matched-pair data. *Stat Med* 2014;33:2612-2633
21. Fleiss J. Measuring nominal scale agreement among many raters. *Psychol Bull* 1971;76:378-382
22. Lee H, Kim B, Kim KJ, Seo J, Park S, Shin YG, et al. Introduction of heat map to fidelity assessment of compressed CT images. *Med Phys* 2011;38:4667-4671
23. Gould MK, Donington J, Lynch WR, Mazzone PJ, Midthun DE, Naidich DP, et al. Evaluation of individuals with pulmonary nodules: when is it lung cancer? Diagnosis and management of lung cancer, 3rd ed: American College of chest physicians evidence-based clinical practice guidelines. *Chest* 2013;143(5 Suppl):e93S-e120S
24. Naidich DP, Bankier AA, MacMahon H, Schaefer-Prokop CM, Pistolesi M, Goo JM, et al. Recommendations for the management of subsolid pulmonary nodules detected at CT: a statement from the Fleischner Society. *Radiology* 2013;266:304-317
25. Lee CT. What do we know about ground-glass opacity nodules in the lung? *Transl Lung Cancer Res* 2015;4:656-659
26. Lee SM, Park CM, Goo JM, Lee HJ, Wi JY, Kang CH. Invasive pulmonary adenocarcinomas versus preinvasive lesions appearing as ground-glass nodules: differentiation by using CT features. *Radiology* 2013;268:265-273
27. Sun H, Wang W. Differentiating between subsolid and solid pulmonary nodules at CT: what is our main task? *Radiology* 2016;281:976-978
28. Vardhanabhuti V, Loader RJ, Mitchell GR, Riordan RD, Roobottom CA. Image quality assessment of standard-and low-dose chest CT using filtered back projection, adaptive statistical iterative reconstruction, and novel model-based iterative reconstruction algorithms. *AJR Am J Roentgenol* 2013;200:545-552
29. Katsura M, Matsuda I, Akahane M, Yasaka K, Hanaoka S, Akai H, et al. Model-based iterative reconstruction technique for ultralow-dose chest CT: comparison of pulmonary nodule detectability with the adaptive statistical iterative reconstruction technique. *Invest Radiol* 2013;48:206-212